2 Fundamental Aspects

2.1 Basic Properties

Some of the basic characteristics of titanium and its alloys are listed in Table 2.1 and compared to those of other structural metallic materials based on Fe, Ni, and Al. Although titanium has the highest strength to density ratio it is the material of choice only for certain niche application areas because of its high price. This high price is mainly a result of the high reactivity of titanium with oxygen. The use of inert atmosphere or vacuum is required during the production process of titanium sponge from titanium tetrachloride as well as during the melting process. Additional major cost elements are energy and the initial high cost of titanium tetrachloride. On the other hand, the high reactivity with oxygen leads to the immediate formation of a stable and adherent oxide surface layer when exposed to air, resulting in the superior corrosion resistance of titanium in various kinds of aggressive environments, especially in aqueous acid environments. The much higher melting temperature of titanium as compared to aluminum, the main competitor in light weight structural applications, gives titanium a definite advantage above application temperatures of about 150°C. The high reactivity of titanium with oxygen limits the maximum use temperature of titanium alloys to about 600°C. Above this temperature the diffusion of oxygen through the oxide surface layer becomes too fast resulting in excessive growth of the oxide layer and embrittlement of the adjacent oxygen rich layer of the titanium alloy (see Sect. 2.9.3).

Table 2.1. Some important characteristics of titanium and titanium based alloys as compared to other structural metallic materials based on Fe, Ni, and Al

	Ti	Fe	Ni	Al
Melting Temperature (°C)	1670	1538	1455	660
Allotropic Transformation (°C)	$\beta \xrightarrow{882} \alpha$	$\gamma \xrightarrow{912} \alpha$	-	-
Crystal Structure	bcc → hex	fcc → bcc	fcc	fcc
Room Temperature E (GPa)	115	215	200	72
Yield Stress Level (MPa)	1000	1000	1000	500
Density (g/cm^3)	4.5	7.9	8.9	2.7
Comparative Corrosion Resistance	Very High	Low	Medium	High
Comparative Reactivity with Oxygen	Very High	Low	Low	High
Comparative Price of Metal	Very High	Low	High	Medium

2.2 Crystal Structure

Pure titanium exhibits an allotropic phase transformation at 882°C, changing from a body-centered cubic crystal structure (β phase) at higher temperatures to a hexagonal close-packed crystal structure (α phase) at lower temperatures. The exact transformation temperature is strongly influenced by interstitial and substitutional elements and therefore depends on the purity of the metal. The hexagonal unit cell of the α phase is shown in Fig. 2.1 indicating also the room temperature values of the lattice parameters a (0.295 nm) and c (0.468 nm). The resulting c/a ratio for pure α titanium is 1.587, smaller than the ideal ratio of 1.633 for the hexagonal close-packed crystal structure. Also indicated in Fig. 2.1 are the three most densely packed types of lattice planes, the (0002) plane, also called basal plane, one of the three $\{10\bar{1}0\}$ planes, also called prismatic planes, and one of the six $\{10\bar{1}1\}$ planes, also called pyramidal planes. The three a_1, a_2, and a_3 axes are the close-packed directions with the indices $<11\bar{2}0>$. The unit cell of the body-centered cubic (bcc) β phase is illustrated in Fig. 2.2 indicating also one variant of the six most densely packed $\{110\}$ lattice planes and the lattice parameter value of pure β titanium at 900°C (a = 0.332 nm). The close-packed directions are the four $<111>$ directions.

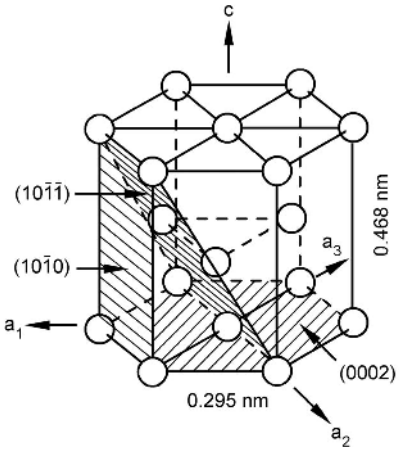

Fig. 2.1. Unit cell of α phase

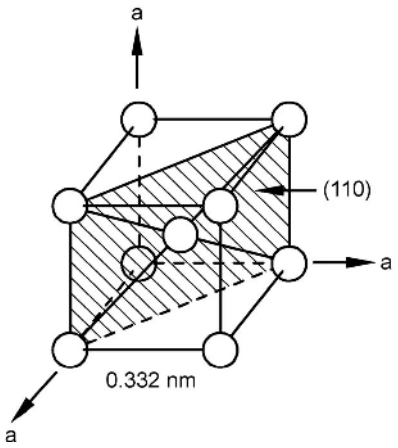

Fig. 2.2. Unit cell of β phase

2.3 Elastic Properties

The intrinsically anisotropic character of the hexagonal crystal structure of the α phase has important consequences for the elastic properties of titanium and its

alloys. The variation of the modulus of elasticity E of pure α titanium single crystals at room temperature as a function of the angle γ between the c-axis of the unit cell and the stress axis is shown in Fig. 2.3 [2.1]. It can be seen that the modulus of elasticity E varies between 145 GPa (stress axis parallel to the c-axis) and 100 GPa (stress axis perpendicular to the c-axis). Similar strong variations are observed for the shear modulus G of single crystals varying between 46 GPa and 34 GPa for shear stresses applied in $<11\bar{2}0>$ direction and in (0002) or $\{10\bar{1}0\}$ planes, respectively. Less pronounced variations in elastic properties are observed in polycrystalline α titanium with crystallographic texture. The actual variations in modulus depend on the nature and intensity of the texture.

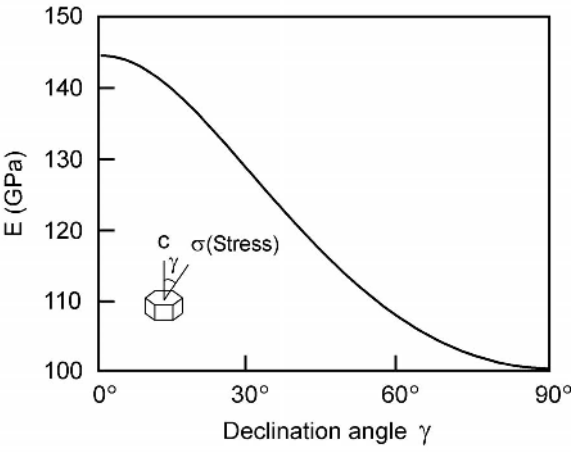

Fig. 2.3. Modulus of elasticity E of α titanium single crystals as a function of declination angle γ [2.1]

With increasing temperature the modulus of elasticity (E) and the shear modulus (G) decrease almost linearly as shown in Fig. 2.4 for polycrystalline texture-free α titanium [2.2]. It can be seen that E drops from about 115 GPa at room temperature to about 58 GPa at the β transus temperature, while G is decreasing from about 42 to 20 GPa over the same temperature range.

The modulus of elasticity of the β phase at room temperature cannot be measured for pure titanium because the β phase is not stable. In binary titanium alloys containing sufficiently high concentrations of β stabilizing elements, for example Ti-V alloys with about 20% vanadium, the metastable β phase can be retained to room temperature by fast cooling (see Sect. 2.5). Modulus data for Ti-V alloys in the water quenched condition are shown in Fig. 2.5 [2.3]. The modulus composition dependence can be discussed in three parts: 0-10% V, 10-20% V, and 20-50% V. From Fig. 2.5, it can be seen that the E value of the β phase increases with increasing vanadium content between 20 and 50% vanadium with a value as low as 85 GPa for 20% V. This shows that the β phase in general has a lower modulus

of elasticity than the α phase. The unusual maximum in E at about 15% vanadium is related to the so-called athermal ω phase formation (see Sect. 2.6.1). The steep decline in modulus from 0-10% V is typical for titanium martensite containing β stabilizing elements. Both the minimum and the maximum in the concentration dependence of E disappear upon annealing in the (α+β) phase field (dashed line in Fig. 2.5) and the modulus follows a tie-line between the (α+β) phase field boundaries, as would be expected from the rule of mixtures. Similar concentration dependences of E have been observed for Ti-Mo, Ti-Nb, and other binary alloys involving β stabilizing elements [2.3]. A commonly used explanation for the steep decline in modulus for martensite containing β stabilizing elements (0-10% range in Fig. 2.5) is the presence of retained metastable β phase which transforms during loading to stress-induced martensite, leading to an apparent low modulus of elasticity of the material [2.4]. But, as recently shown [2.5], a Ti-7Mo alloy exhibiting the low E value of 72 GPa was 100% martensitic and did not contain any retained metastable β phase. So, the steep decline in modulus seems to result directly from the fact that the β stabilizing elements severely disturb and reduce the bonding force of the lattice. It is interesting to note, that the martensite in some of these alloys also shows the tendency for spinodal decomposition (see Sect. 2.6.1). In contrast, the most common α stabilizing element (aluminum) increases the modulus of elasticity of the α phase [2.6]. For solid solutions this concentration dependence of E is atypical. In the case of the Ti-Al system, it seems to be related to the tendency of ordering (see Sect. 2.5) with a concomitant increase in covalent bonding.

In general, commercial β titanium alloys have lower E values than α and α+β alloys. Typical values are 70-90 GPa for the as-quenched condition and 100-105 GPa for the annealed condition of commercial β alloys, 105 GPa for CP titanium, and about 115 GPa for commercial α+β alloys [2.7].

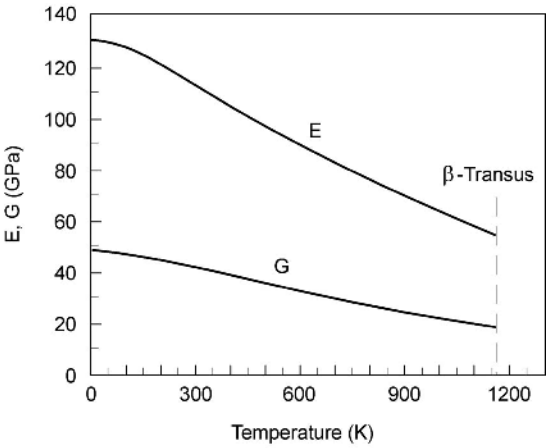

Fig. 2.4. Modulus of elasticity E and shear modulus G as a function of temperature of α titanium polycrystals [2.2]

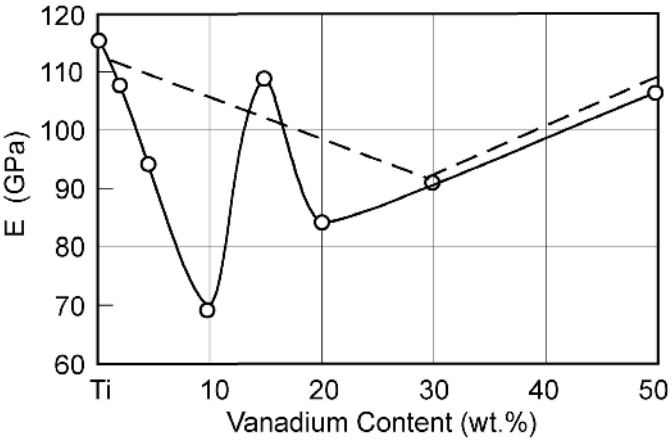

Fig. 2.5. Modulus of elasticity E of Ti-V alloys, solid line: 24h 900°C/WQ, dashed line: annealed at 600°C [2.3]

2.4 Deformation Modes

The ductile behavior of hexagonal α titanium, especially at low temperatures, results from the activation of twinning deformation modes in addition to conventional slip by dislocations. These twinning modes are important for the deformation behavior of CP titanium and some α titanium alloys. Although twinning is suppressed nearly completely in two phase α+β alloys by the small phase dimensions, high solute content, and presence of Ti_3Al precipitates, these alloys are quite ductile at low temperatures due to their small phase dimensions.

The bcc β phase also shows twinning in addition to slip but the occurrence of twinning in β alloys is limited again to the single phase state and decreases with increasing solute content. In fully heat treated β alloys, which are hardened by the precipitation of α particles, twinning is completely suppressed. In these alloys twinning might occur during the forming operations prior to aging. Some commercial β alloys also can form deformation induced martensite which further enhances their formability (see Sect. 2.6.1). Formation of this deformation induced martensite is very sensitive to alloy composition.

2.4.1 Slip Modes

The various slip planes and slip directions for α titanium are indicated in the hexagonal unit cell in Fig. 2.6. The main slip directions are the three close-packed directions of the type $<11\bar{2}0>$. The slip planes containing this $\vec{a}$ type of Burgers vector are the (0002) plane, the three $\{10\bar{1}0\}$ planes, and the six $\{10\bar{1}1\}$ planes. Among these three different types of slip planes together with the possible slip

directions there are a total of 12 slip systems (Table 2.2) [2.8, 2.9]. These can be reduced to nominally 8 independent slip systems. However, this number is further reduced to only 4 independent slip systems because the shape changes that are produced by the combined action of slip system types 1 and 2 (see Table 2.2) are exactly the same as those of slip system type 3. Therefore, assuming the von Mises criterion is correct, which requires at least five independent slip systems for a homogenous plastic deformation of polycrystals, the operation of one of the slip systems with a so-called non-basal Burgers vector needs to be activated, either the $\vec{c}$ type with the slip direction $[0001]$ or the $\vec{c}+\vec{a}$ type with the slip direction $<11\bar{2}3>$ (see Fig. 2.6 and Table 2.2). The presence of $\vec{c}+\vec{a}$ type dislocations has been observed by TEM observations in a number of titanium alloys [2.10, 2.11]. To justify the presence of these $\vec{c}+\vec{a}$ dislocations it is not so important whether the von Mises criterion is valid or not, but rather to answer the question which slip systems are activated if a grain in a polycrystalline material is orientated such that the applied stress is parallel to the c-axis. In that case, neither a slip system with an $\vec{a}$ Burgers vector nor dislocations with a $\vec{c}$ Burgers vector can be activated because the Schmidt factor for both is zero. From the possible slip planes of the dislocations with a $\vec{c}+\vec{a}$ Burgers vector, the $\{10\bar{1}0\}$ slip planes cannot be activated because they are parallel to the stress axis and from the other possible slip planes (see Figure 2.6) the $\{11\bar{2}2\}$ planes are closer to 45° (higher Schmidt factor) than the $\{10\bar{1}1\}$ planes. Assuming the critical resolved shear stresses (CRSS) are about the same for both types of slip planes, then the slip system with a non-basal Burgers vector which is activated most likely in α titanium is of the type $<11\bar{2}3>$ $\{11\bar{2}2\}$, shown in Table 2.2 as slip system type 4.

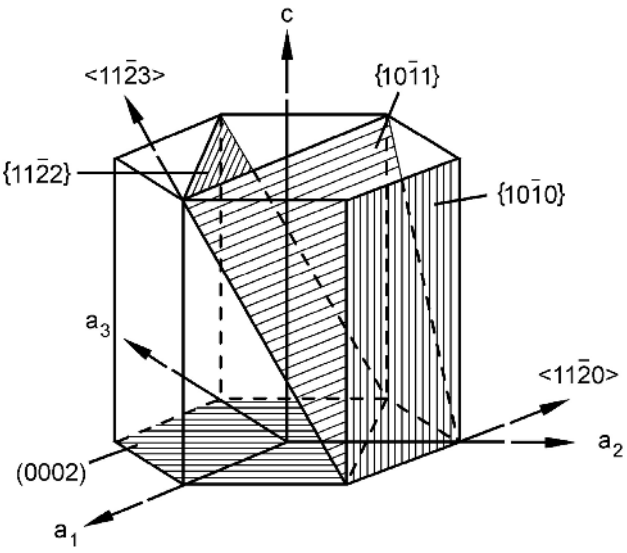

Fig. 2.6. Slip planes and slip directions in the hexagonal α phase

Table 2.2. Slip systems in the hexagonal α phase [2.8, 2.9]

Slip system type	Burgers vector type	Slip direction	Slip plane	No. of slip systems Total	Independent
1	$\vec{a}$	$<11\bar{2}0>$	(0002)	3	2
2	$\vec{a}$	$<11\bar{2}0>$	$\{10\bar{1}0\}$	3	2
3	$\vec{a}$	$<11\bar{2}0>$	$\{10\bar{1}1\}$	6	4
4	$\vec{c}+\vec{a}$	$<11\bar{2}3>$	$\{11\bar{2}2\}$	6	5

Taking into account the large difference in CRSS between $\vec{c}+\vec{a}$ slip and $\vec{a}$ slip, which was measured for Ti-6.6Al single crystals (Fig. 2.7) [2.12], the percentage of grains deforming by $\vec{c}+\vec{a}$ slip will be quite low in α titanium polycrystals without crystallographic texture, because the activation of $\vec{a}$ slip is easier even for an angle of about 10° between the stress axis and the c-axis.

The absolute values of the CRSS are strongly dependent on alloy content and on test temperature (Fig. 2.7). The small differences in CRSS at room temperature between the three types of slip systems with a basal ($\vec{a}$ type) Burgers vector, $\{10\bar{1}0\} < \{10\bar{1}1\} < (0002)$, become even smaller with increasing temperature (Fig. 2.7).

As shown for binary Ti-V alloys [2.13], the slip systems in bcc β titanium alloys are $\{110\}$, $\{112\}$, and $\{123\}$, all with the same Burgers vector of the type $<111>$, in agreement with the generally observed slip modes in bcc metals.

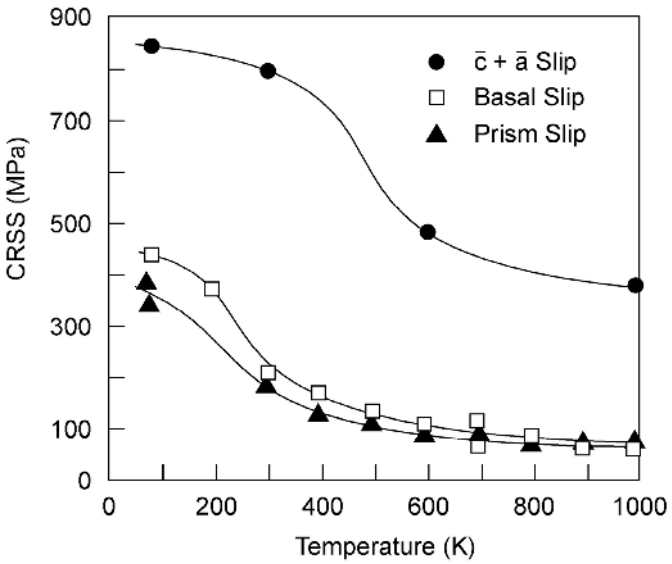

Fig. 2.7. Temperature dependence of CRSS for slip with $\vec{a}$ and $\vec{c}+\vec{a}$ Burgers vectors in single crystals of Ti-6.6Al [2.12]

2.4.2 Deformation Twinning

The main twinning modes observed in pure α titanium are $\{10\bar{1}2\}$, $\{11\bar{2}1\}$, and $\{11\bar{2}2\}$. The crystallographic elements of these three twin systems in α titanium are listed in Table 2.3 [2.8]. Twinning modes are especially important for plastic deformation and ductility at low temperatures if the stress axis is parallel to the c-axis and the dislocations with a basal Burgers vector cannot move. In this case, $\{10\bar{1}2\}$ and $\{11\bar{2}1\}$ twins are activated during deformation in tension leading to an extension along the c-axis. The most frequently observed twins are of the $\{10\bar{1}2\}$ type but they have the smallest twinning shear (Table 2.3). The shape change associated with a $\{11\bar{2}1\}$ twin having a much larger magnitude of twinning shear is shown in Fig. 2.8 [2.8]. Under compression loading parallel to the c-axis $\{11\bar{2}2\}$ twins are activated allowing a contraction along the c-axis (Fig. 2.9) [2.8]. After compression loading, $\{10\bar{1}1\}$ twins were also observed but only at relatively high deformation temperatures above 400°C [2.14].

Increasing concentrations of solute atoms in α titanium, such as oxygen or aluminum, suppress the occurrence of twinning. Therefore, twinning as a deformation mode to allow shape changes parallel to the c-axis only plays a major role in pure titanium or in CP titanium with low oxygen concentrations [2.10].

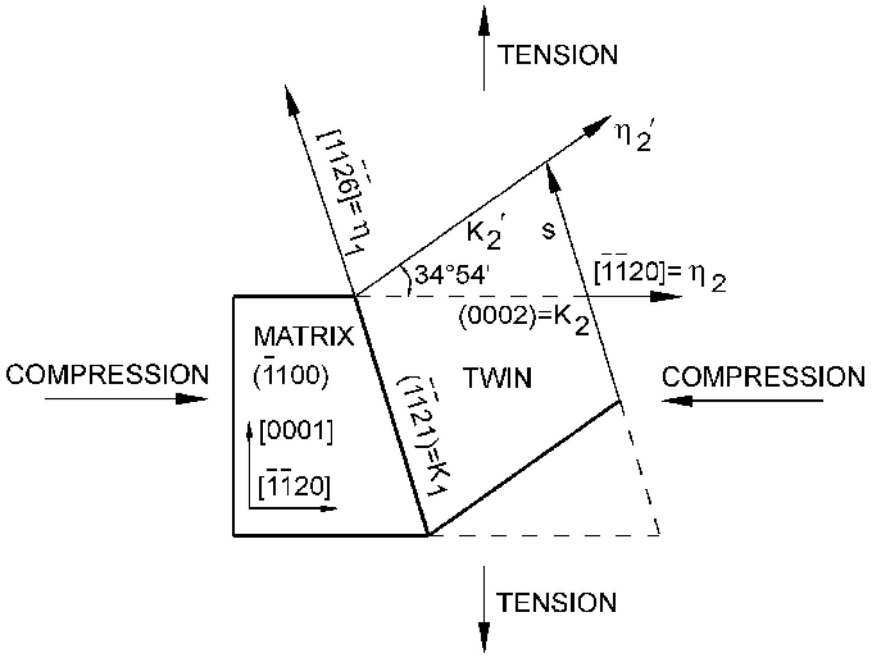

Fig. 2.8. Shape change by $\{11\bar{2}1\}$ twinning [2.8]

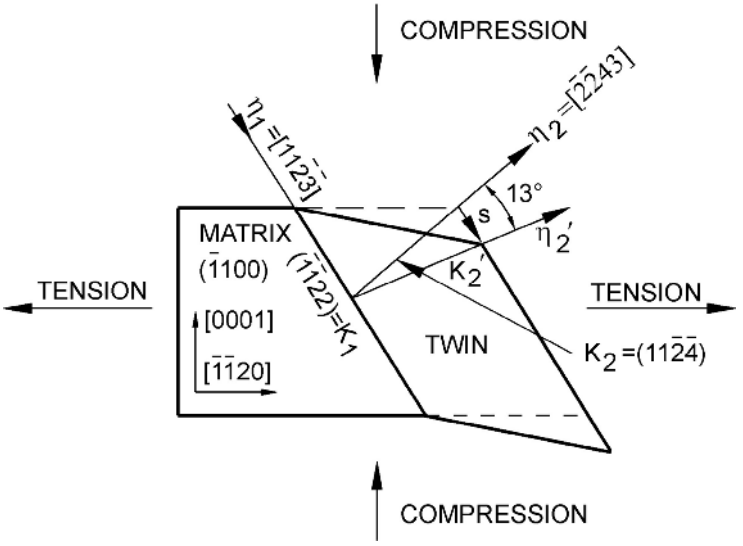

Fig. 2.9. Shape change by $\{ 11\bar{2}2 \}$ twinning [2.8]

Table 2.3. Twinning elements in α titanium [2.8]

Twinning plane (1st undeformed plane) (K_1)	Twinning shear direction (η_1)	Second undeformed plane (K_2)	Direction of intersection of plane of shear with K_2 (η_2)	Plane of shear perpendicular to K_1 and K_2	Magnitude of twinning shear
$\{10\bar{1}2\}$	$<10\bar{1}\bar{1}>$	$\{\bar{1}012\}$	$<10\bar{1}1>$	$\{1\bar{2}10\}$	0.167
$\{11\bar{2}1\}$	$<11\bar{2}\bar{6}>$	(0002)	$<11\bar{2}0>$	$\{\bar{1}100\}$	0.638
$\{11\bar{2}2\}$	$<11\bar{2}3>$	$\{11\bar{2}\bar{4}\}$	$<22\bar{4}3>$	$\{\bar{1}100\}$	0.225

2.5 Phase Diagrams

Alloying elements in titanium are usually classified into α or β stabilizing additions depending on whether they increase or decrease the α/β transformation temperature of 882°C of pure titanium.

The substitutional element Al and the interstitial elements O, N, and C are all strong α stabilizers and increase the transus temperature with increasing solute content, as can be seen from the schematic phase diagram in Fig. 2.10. Aluminum is the most widely used alloying element in titanium alloys, because it is the only common metal raising the transition temperature and having large solubilities in both the α and β phases. Among the interstitial elements, oxygen can be consid-

ered as an alloying element in titanium in those cases where the oxygen content is used to obtain the desired strength level. This is especially true for the different grades of CP titanium. Other α stabilizers include B, Ga, Ge, and the rare earth elements but their solid solubilities are much lower as compared to aluminum or oxygen and none of these elements is used commonly as an alloying element.

The β stabilizing elements are divided into β isomorphous elements and β eutectoid forming elements, depending on the details of the resulting binary phase diagrams. Both types of phase diagrams are shown schematically in Fig. 2.10. The most frequently used β isomorphous elements in titanium alloys are V, Mo, and Nb. Sufficient concentrations of these elements make it possible to stabilize the β phase to room temperature. Other elements belonging to this group that are rarely used or not used at all because of density considerations, are Ta and Re. From the β eutectoid forming elements, Cr, Fe, and Si are used in many titanium alloys, whereas Ni, Cu, Mn, W, Pd, and Bi have only very limited usage. These elements are used only in one or two special purpose alloys. Other β eutectoid forming elements, such as Co, Ag, Au, Pt, Be, Pb, and U, are not used at all in titanium alloys. It should be mentioned, that hydrogen belongs to these β eutectoid forming elements and that the low eutectoid temperature of 300°C in combination with the high diffusivity of hydrogen led to a special process of microstructure refinement, the so-called hydrogenation/dehydrogenation (HDH) process. HDH uses hydrogen as a temporary alloying element, see Sect. 3.5.2. Generally, the maximum hydrogen content in CP titanium and titanium alloys is strictly limited to about 125-150 ppm because of hydrogen embrittlement.

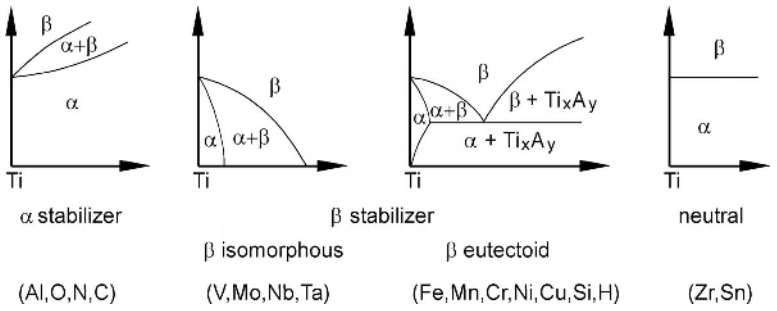

Fig. 2.10. Effect of alloying elements on phase diagrams of titanium alloys (schematically)

In addition, there exist some elements (Zr, Hf and Sn) which behave more or less neutrally (Fig. 2.10), because they lower the α/β transformation temperature only slightly and then increase the transformation temperature again at higher concentrations. Zr and Hf are isomorphous with titanium and, therefore, both exhibit the same β to α allotropic phase transformation. These elements have complete solubilities in the α and β phases of titanium. In contrast, Sn belongs to the β eutectoid forming elements, but has essentially no effect on the α/β transformation temperature. Many commercial multicomponent alloys contain Zr and

Sn but in these alloys both elements are considered and counted as α stabilizing elements. This is because of the chemical similarity of Zr to titanium and because Sn can replace aluminum in the hexagonal ordered Ti_3Al phase (α_2). When present with aluminum, Sn behaves as α stabilizer. This example shows that the interactions between alloying elements make it difficult to understand titanium alloying behavior on the basis of binary Ti-X systems. Rosenberg [2.15] attempted to express the effect of α stabilizing elements in multicomponent titanium alloys as an equivalent aluminum content by establishing the following equation: $[Al]_{eq.} = [Al] + 0.17\,[Zr] + 0.33\,[Sn] + 10\,[O]$.

A more detailed description of the influence of the various alloying elements on the stability of the α and β phases taking into account electronic and thermodynamic considerations can be found in a summary article by Collings [2.6].

Although all binary equilibrium phase diagrams of titanium are included in the ASM Handbook on Alloy Phase Diagrams [2.16], a few of the most important ones will be shown as illustrations and discussed briefly in the following section.

As already pointed out above, aluminum is the most important α stabilizer and is therefore present in many titanium alloys. The binary Ti-Al phase diagram (Fig. 2.11) shows that with increasing aluminum content the Ti_3Al (α_2) phase will be formed and that the two phase region ($\alpha+Ti_3Al$) starts at about 5% Al for a temperature of about 500°C. To avoid any appreciable amount of coherent Ti_3Al precipitates in the α phase, the aluminum content in most titanium alloys is limited to about 6%. From Fig. 2.11 it can be seen that for this aluminum level of about 6% the α/β transformation temperature of 882°C for pure titanium is increased to about 1000°C for the two phase region (α+β). In addition to conventional titanium alloys, the Ti-Al phase diagram is also the basis for the so-called titanium-aluminides, which are recently developed alloys based on the two intermetallic compounds Ti_3Al (Alpha-2 alloys and the orthorhombic variant, Ti_2AlNb alloys) and TiAl (Gamma alloys), see Chap. 8.

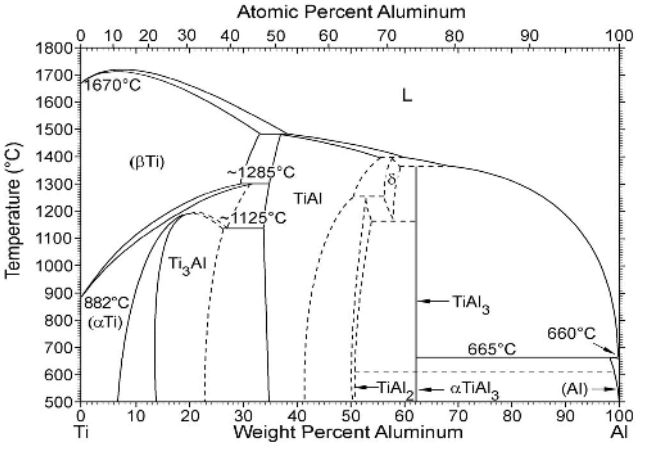

Fig. 2.11. Ti-Al phase diagram [2.16]

From the three most important β isomorphous elements (V, Mo, and Nb) the Ti-Mo binary phase diagram is selected (Fig. 2.12). This is because it is convenient to calculate an equivalent molybdenum content (as in case of an equivalent aluminum content) for all β stabilizers in multicomponent titanium alloys (see Sect. 2.6.1). For the phase diagram in Fig. 2.12 the older version, published 1958 in the 2nd edition of the Hansen book on Constitution of Binary Alloys [2.17], is taken rather than the newer version [2.16] which exhibits a miscibility gap above 20% Mo, in which the β phase separates into two bcc phases (β'+β) outside the (α+β) phase field. The maximum molybdenum content present in conventional titanium alloys is about 15%, so the miscibility gap only adds complexity to the present discussion without helping to understand the effects of alloying additions in the concentration ranges of interest. Indeed, it can be seen from Fig. 2.12 that 15% Mo lowers the β → α+β transformation temperature from 882°C for pure titanium to about 750°C. Furthermore, it can be seen from Fig. 2.12 that the solid solubility of Mo in the α phase is very low (below 1%). The Ti-V and Ti-Nb phase diagrams are qualitatively similar to Fig. 2.12. By adding 15% V, which is also about the maximum vanadium content in conventional titanium alloys, the β → α+β transformation temperature is lowered to about 700°C. The maximum solid solubility of V in the α phase is at 680°C about 3% and therefore much higher as compared to molybdenum. The addition of Nb in conventional titanium alloys is kept within the range of 1-3%, much lower than the maximum amounts of Mo and V. The influence of Nb on the β → α+β transformation temperature is similar to Mo, the transus is lowered to about 750°C by an addition of 15% Nb.

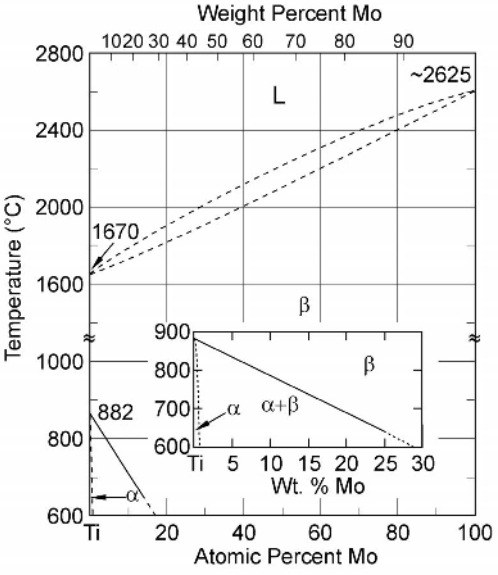

Fig. 2.12. Ti-Mo phase diagram [2.17]

Among the β eutectoid forming elements, the Ti-Cr binary phase diagram has been chosen and is shown in Fig. 2.13. It can be seen that Cr is an effective β stabilizing element, the eutectoid temperature being 667°C and the eutectoid point lying at about 15% Cr. It is important that the eutectoid decomposition is very sluggish, so that in conventional titanium alloys with Cr contents below 5% the precipitation of the intermetallic compound $TiCr_2$ is avoided. The only exception is the old B120VCA alloy with 11% Cr used in the SR-71 airplane (see Sect. 1.3). This alloy is unstable because it forms $TiCr_2$ precipitates after prolonged exposure to elevated temperatures. This instability is accompanied by a severe loss in ductility. In general, this experience has led to the desire to avoid the formation of the eutectoid compound in this class of alloys. A characteristic of all β eutectoid forming elements is a low solid solubility in the α phase. For example, in the Ti-Cr system (Fig. 2.13) the maximum solubility is only about 0.5%. Consequently, nearly all of the β eutectoid forming element additions partition to the β phase. A second commonly used β eutectoid forming element is Fe which is even a stronger β stabilizing element than chromium, the eutectoid temperature in the Ti-Fe system being about 600°C. The formation of the equilibrium intermetallic compound is avoided in commercial titanium alloys with Fe additions up to a maximum of 5.5% as verified in the recently developed TIMET alloy "low cost beta" (LCB), Ti-1.5Al-5.5Fe-6.8Mo. An exception, where the presence of the compound is desirable, is the β eutectoid forming element Si, which is a common addition to titanium alloys for high temperature application. In this case, the precipitation of the intermetallic compound Ti_5Si_3 is deliberately used for the improvement of creep properties (see Sect. 6.2).

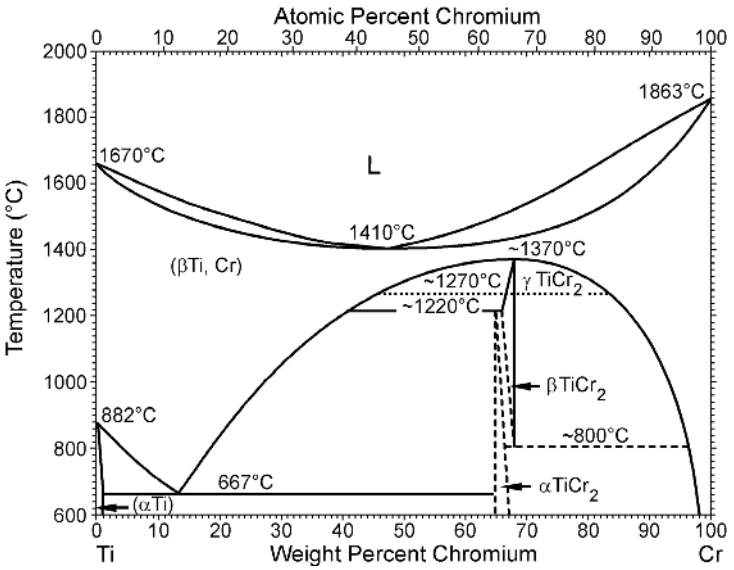

Fig. 2.13. Ti-Cr phase diagram [2.16]

It should be emphasized, however, that most commercial titanium alloys are multicomponent alloys. As mentioned earlier, the binary phase diagrams can serve only as a qualitative guideline. In principle, ternary or quaternary phase diagrams should be used. This is illustrated in Fig. 2.14 showing isothermal sections through the Ti-rich corner of the Ti-Al-V system at 1000°C, 900°C, and 800°C [2.6]. In practice, not all the necessary higher order phase diagrams have been determined and judicious use of binary diagrams is the only choice the metallurgists have.

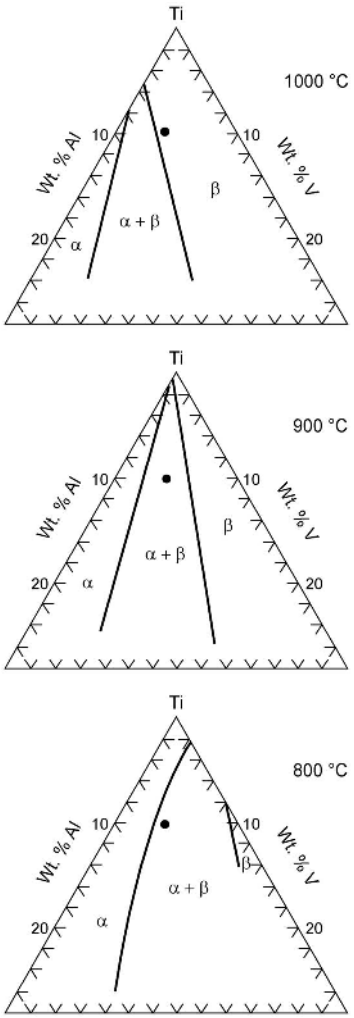

Fig. 2.14. Isothermal sections at 1000°C, 900°C, and 800°C through the Ti-rich corner of the ternary Ti-Al-V phase diagram (solid point: Ti-6Al-4V) [2.6]

2.6 Phase Transformations

The transformation of the bcc β phase to the hexagonal α phase in CP titanium and titanium alloys can occur martensitically or by a diffusion controlled nucleation and growth process depending on cooling rate and alloy composition. The crystallographic orientation relationship between α and β has first been studied for zirconium by Burgers [2.18] and is therefore named the Burgers relationship:

$$(110)_\beta \parallel (0002)_\alpha$$
$$[1\bar{1}1]_\beta \parallel [11\bar{2}0]_\alpha$$

This relationship was confirmed later also for titanium [2.19]. According to this relationship, a bcc crystal can transform to 12 hexagonal variants, having different orientations with regard to the parent β crystal. This Burgers relationship is closely obeyed for both the martensite transformation and the conventional nucleation and growth process.

2.6.1 Martensite Transformation

The martensite transformation involves the cooperative movement of atoms by a shear type process resulting in a microscopically homogeneous transformation of the bcc into the hexagonal crystal lattice over a given volume. The transformed volume is usually plate shaped or better described geometrically as disk shaped for most titanium alloys. The entire shear transformation process can be reduced to the activation of the following shear systems [2.20]: $[111]_\beta\ (11\bar{2})_\beta$ and $[111]_\beta\ (\bar{1}01)_\beta$ or in hexagonal notation: $[2\bar{1}\bar{1}3]_\alpha\ (\bar{2}112)_\alpha$ and $[2\bar{1}\bar{1}3]_\alpha\ (\bar{1}011)_\alpha$. This hexagonal martensite is designated as α' and is observed in two morphologies: massive martensite (other names: lath or packet martensite) and "acicular" martensite [2.21]. Massive martensite occurs only in pure titanium, very dilute alloys, and in alloys with a high martensitic transformation temperature. "Acicular" martensite occurs in alloys with higher solute content (lower martensitic transformation temperature). The massive martensite consists of large irregular regions (size about 50-100 μm) without any clear internal features visible by light microscopy, but these regions contain packets of small, almost parallel α plates or laths (thickness about 0.5-1 μm) belonging to the same variant of the Burgers relationship. The "acicular" martensite consists of an intimate mixture of individual α plates, each having a different variant of the Burgers relationship (Fig. 2.15). Generally, the martensitic plates contain a high dislocation density and sometimes twins. The hexagonal α' martensite is supersaturated in β stabilizers and, upon annealing in the (α+β) phase field, decomposes to α+β by precipitating incoherent β particles at dislocations or β phase layers at plate boundaries.

With increasing solute content the hexagonal structure of the martensite becomes distorted and, from a crystallographic viewpoint, the crystal structure loses its hexagonal symmetry and must be described as orthorhombic [2.21]. This orthorhombic martensite is designated α". The α'/α" boundary in terms of solute content is tabulated for some binary titanium systems with transition metals in ta-

ble 2.4 [2.6]. For this orthorhombic martensite, the initial stage of decomposition upon annealing in the (α+β) phase field seems to be a spinodal decomposition in solute lean α" and solute rich α" regions forming a characteristically modulated microstructure [2.22], before finally the β phase is precipitated ($\alpha''_{lean} + \alpha''_{rich} \rightarrow \alpha+\beta$). The martensitic start temperature (M_S) of pure titanium depends on the impurity level (oxygen, iron), but lies around 850°C, and increases with increasing amounts of α stabilizers, such as aluminum and oxygen, and decreases with increasing β stabilizer content. Table 2.5 shows the solute contents of some transition metals necessary to suppress the M_S-temperature below room temperature [2.6]. Using these values of the binary systems, a quantitative rule describing the individual effects of β stabilizing elements in terms of an equivalent Mo content was generated for multicomponent alloys: $[Mo]_{eq.}$ = [Mo] + 0.2 [Ta] + 0.28 [Nb] + 0.4 [W] + 0.67 [V] + 1.25 [Cr] + 1.25 [Ni] + 1.7 [Mn] + 1.7 [Co] + 2.5 [Fe]. Caution should be exercised if attempting to use this equation quantitatively. However, it is a useful qualitative tool which, together with the equivalent Al content derived by Rosenberg [2.15] (see Sect. 2.5), permits the evaluation of the expected constitution of an alloy with a given chemistry.

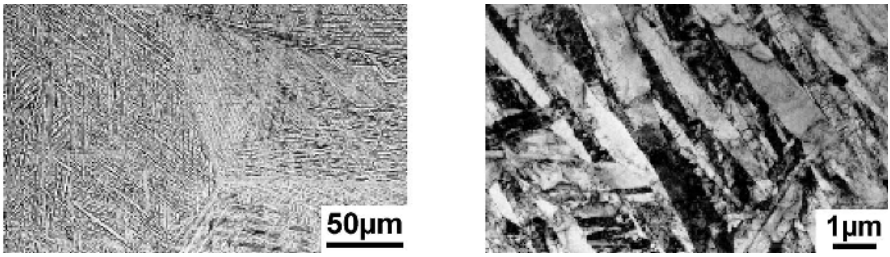

a b

Fig. 2.15. "Acicular" martensite in Ti-6Al-4V quenched from the β phase field: (a) LM (b) TEM

Although not being relevant to any practical application of titanium alloys, it should be mentioned that in many alloys in which the martensitic reaction is suppressed, the β phase decomposes upon quenching athermally to the so-called athermal ω phase. The athermal ω phase forms as uniform dispersion of extremely fine particles (size 2-4 nm). These have been suggested to be a precursor to the martensitic reaction because the athermal transformation involves a shear displacement in the <111> direction of the bcc lattice, see Fig. 2.16 [2.6] showing the (222) planes of the bcc lattice. From a crystallographic viewpoint, the athermal ω phase has a trigonal symmetry in heavily β stabilized alloys and a hexagonal symmetry (not hexagonal close-packed) in leaner alloys. The transition from hexagonal to trigonal is continuous as a function of alloy content. From a standpoint of dislocation movement in the bcc β structure, the ω particles have a diffuse, coherent interface and the structure is an elastically distorted bcc lattice, i.e. moving dislocations in the β phase can cut all four variants of ω particles. Upon annealing in the metastable (ω+β) phase field, the athermal ω phase grows to form

the so-called isothermal ω phase which has the same crystallographic symmetry as the athermal ω but is solute lean with respect to the β phase, see Sect. 2.8.2.

Table 2.4. Composition of the α'/α" (hexagonal/orthorhombic) martensite boundary in some binary titanium systems with transition metals [2.6]

α'/α" Boundary	V	Nb	Ta	Mo	W
Wt%	9.4	10.5	26.5	4	8
At%	8.9	5.7	8.7	2.0	2.2

Table 2.5. Concentration of some transition metals needed to retain the β phase at room temperature in binary titanium alloys [2.6]

	V	Nb	Ta	Cr	Mo	W	Mn	Fe	Co	Ni
Wt%	15	36	50	8	10	25	6	4	6	8
At%	14.2	22.5	20.9	7.4	5.2	8	5.3	3.4	4.9	6.6

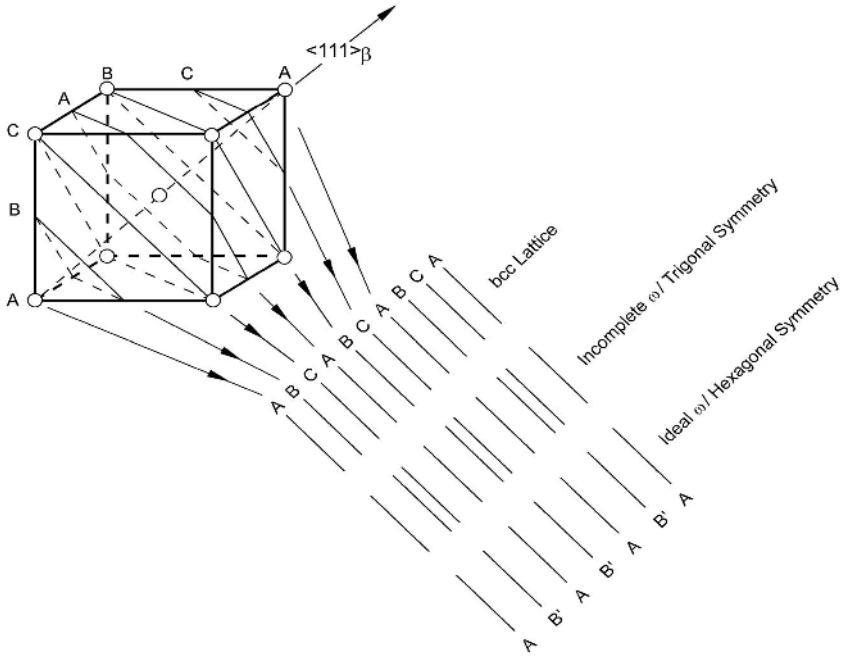

Fig. 2.16. Representation of the β → ω transformation showing the (222) planes of the bcc lattice [2.6]

2.6.2
Nucleation and Diffusional Growth

When titanium alloys are cooled at sufficiently low rates from the β phase field into the (α+β) phase field, the α phase, which is incoherent with respect to the β phase, first nucleates preferentially at β grain boundaries leading to a more or less continuous α layer along β grain boundaries. During continued cooling α plates nucleate either at the interface of the continuous α layer or at the β grain boundary itself and grow into the β grain as parallel plates [2.23] belonging to the same variant of the Burgers relationship (so-called α colony). They continue to grow into the β grain interior until they meet other α colonies nucleated at other grain boundary areas of the β grain and belonging to other variants of the Burgers relationship. This process is often called sympathetic nucleation and growth. The individual α plates are separated within the α colonies by the retained β matrix, which are commonly, but incorrectly, called β plates. The α and β plates are also often called α and β lamellae and the resulting microstructure is then designated as lamellar. An example of such a microstructure which was obtained by slow cooling from the β phase field is shown in Fig. 2.17 for the Ti-6Al-4V alloy. In such slowly cooled material, the size of the α colonies can be as large as half of the β grain size.

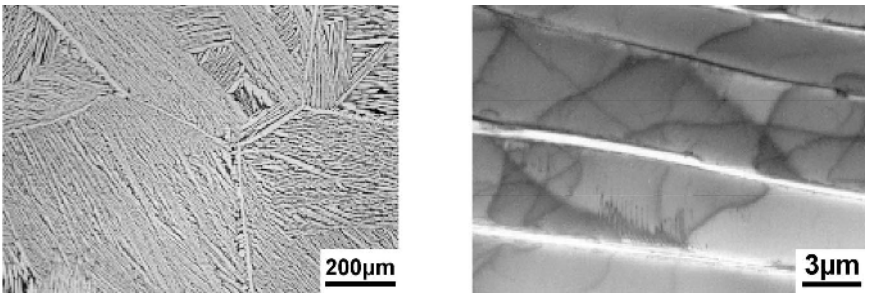

a b

Fig. 2.17. Lamellar α+β microstructure in Ti-6Al-4V slowly cooled from the β phase field: (a) LM (b) TEM

The crystallographic relationship between α and β plates within a colony is schematically shown in Fig. 2.18. It can be seen that the Burgers relationship $(110)_\beta \parallel (0002)_\alpha$ and $[1\bar{1}1]_\beta \parallel [11\bar{2}0]_\alpha$ is strictly obeyed and that the flat surface of the α plates is parallel to the $(\bar{1}100)$ plane of the α phase and parallel to the $(\bar{1}12)$ plane of the β phase. It should be pointed out again, that these flat surfaces are nearly equiaxed shaped (disk shaped) and the diameter is usually called α plate length.

With increasing cooling rate the size of the α colonies as well as the thickness of the individual α plates become smaller. Colonies nucleated at β grain boundaries cannot fill the whole grain interior anymore and colonies start to nucleate also on boundaries of other colonies. To minimize the overall elastic strains, the new α

plates nucleating by "point" contact on the broad face of an existing α plate tend to grow nearly perpendicular to that plate. This selective nucleation and growth mechanism in combination with the smaller number of α plates within the colonies leads to a characteristic microstructure called "basket weave" structure or Widmanstätten structure. For a given cooling rate this type of "basket weave" structure is observed more frequently in alloys with higher contents of β stabilizing elements, especially with slow diffusing elements. It should be mentioned that during continuous cooling from the β phase field the incoherent α plates are not nucleating homogeneously throughout the β matrix.

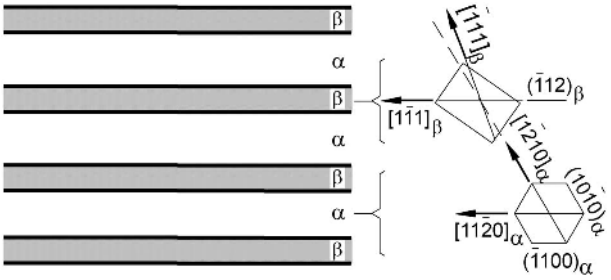

Fig. 2.18. Schematical representation of the crystallographic relationship between α plates and β matrix in α colonies

2.7 Alloy Classification

Commercial titanium alloys are classified conventionally into three different categories (α, α+β, and β alloys) according to their position in a pseudo-binary section through a β isomorphous phase diagram, schematically shown in Fig. 2.19. A list of the most important commercial alloys belonging to each of these three different groups is shown in Table 2.6. In this table the common name, the nominal composition, and the nominal β transus temperature are stated for each alloy.

The group of alloys called α alloys in Table 2.6 consists of the various grades of CP titanium and α alloys which upon annealing well below the β transus contain only small amounts of β phase (2-5 vol%) stabilized by iron. The β phase is helpful in controlling the recrystallized α grain size and improves the hydrogen tolerance of these alloys. The four different grades of CP titanium differ with respect to their oxygen content from 0.18% (grade 1) to 0.40% (grade 4) in order to increase the yield stress level. The two alloys Ti-0.2Pd and Ti-0.3Mo-0.8Ni offer better corrosion resistance than CP titanium. Their common names are grade 7 and grade 12, respectively, and the iron and oxygen limits are identical to grade 2 of CP titanium. Ti-0.2Pd offers better corrosion resistance but is more expensive than Ti-0.3Mo-0.8Ni. The α alloy Ti-5Al-2.5Sn (0.20% oxygen) has a much higher yield stress level (780-820 MPa) than the CP titanium grades (grade

4: 480 MPa). It can be used at service temperatures up to 480°C and in its ELI (extra low interstitials) version with 0.12% oxygen also at low temperatures (–250°C). It is an old alloy, first manufactured in 1950, but still on the market, although it is being replaced by Ti-6Al-4V in many applications.

Table 2.6. Important commercial titanium alloys

Common Name	Alloy Composition (wt%)	T_β (°C)
α Alloys and CP Titanium		
Grade 1	CP-Ti (0.2Fe, 0.18O)	890
Grade 2	CP-Ti (0.3Fe, 0.25O)	915
Grade 3	CP-Ti (0.3Fe, 0.35O)	920
Grade 4	CP-Ti (0.5Fe, 0.40O)	950
Grade 7	Ti-0.2Pd	915
Grade 12	Ti-0.3Mo-0.8Ni	880
Ti-5-2.5	Ti-5Al-2.5Sn	1040
Ti-3-2.5	Ti-3Al-2.5V	935
α+β Alloys		
Ti-811	Ti-8Al-1V-1Mo	1040
IMI 685	Ti-6Al-5Zr-0.5Mo-0.25Si	1020
IMI 834	Ti-5.8Al-4Sn-3.5Zr-0.5Mo-0.7Nb-0.35Si-0.06C	1045
Ti-6242	Ti-6Al-2Sn-4Zr-2Mo-0.1Si	995
Ti-6-4	Ti-6Al-4V (0.20O)	995
Ti-6-4 ELI	Ti-6Al-4V (0.13O)	975
Ti-662	Ti-6Al-6V-2Sn	945
IMI 550	Ti-4Al-2Sn-4Mo-0.5Si	975
β Alloys		
Ti-6246	Ti-6Al-2Sn-4Zr-6Mo	940
Ti-17	Ti-5Al-2Sn-2Zr-4Mo-4Cr	890
SP-700	Ti-4.5Al-3V-2Mo-2Fe	900
Beta-CEZ	Ti-5Al-2Sn-2Cr-4Mo-4Zr-1Fe	890
Ti-10-2-3	Ti-10V-2Fe-3Al	800
Beta 21S	Ti-15Mo-2.7Nb-3Al-0.2Si	810
Ti-LCB	Ti-4.5Fe-6.8Mo-1.5Al	810
Ti-15-3	Ti-15V-3Cr-3Al-3Sn	760
Beta C	Ti-3Al-8V-6Cr-4Mo-4Zr	730
B120VCA	Ti-13V-11Cr-3Al	700

Classifying titanium alloys by their constitution (α, α+β, and β) is convenient but can be misleading. For example, essentially all α alloys contain a small amount of β phase as mentioned above and as will be discussed in more detail in Chap. 4, Sect. 4.1.1. Perhaps a better criterion for α alloys is the lack of heat

treatment response. Following this criterion, the alloy Ti-3Al-2.5V is best classified as α titanium alloy, as shown in Table 2.6. This alloy which is often called "Half Ti-6-4" has excellent cold formability and is used mainly as seamless tubing in aerospace applications and for sporting goods.

The group of α+β alloys (Table 2.6) has a range in the phase diagram (Fig. 2.19) from the α/α+β phase boundary up to the intersection of the M_S-line with room temperature, thus α+β alloys transform martensitically upon fast cooling from the β phase field to room temperature. Alloys which contain in equilibrium only a small volume fraction of β phase (less than about 10 vol%) are also often called "near α" alloys and their main usage is at high service temperatures. Although they belong per definition to the α+β alloys and are listed in that way in Table 2.6, some special features of these high temperature titanium alloys will be discussed in a separate chapter (Chap. 6) distinguishing them from the common α+β alloys (Chap. 5) dominated by the Ti-6Al-4V alloy. The Ti-6Al-4V alloy contains in equilibrium at 800°C about 15 vol% β phase (see Fig. 2.14). This alloy has an exceptional good balance of strength, ductility, fatigue, and fracture properties but can be used only up to temperatures of about 300°C. The ELI version of this popular alloy has especially high fracture toughness values and excellent damage tolerance properties.

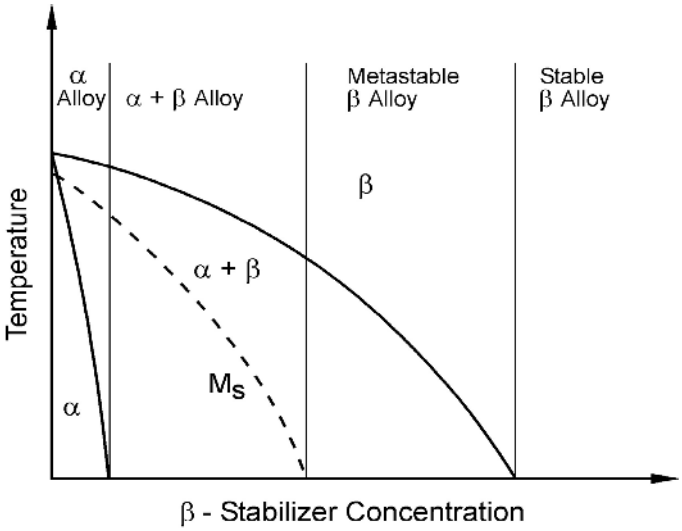

Fig. 2.19. Pseudo-binary section through a β isomorphous phase diagram (schematically)

All alloys in the group of β alloys in Table 2.6 are actually metastable β alloys because they all are located in the equilibrium (α+β) phase region of the phase diagram (Fig. 2.19). Since stable β alloys located in the β single phase field

(Fig. 2.19) do not exist as commercial materials, the expression β alloys is commonly used and also used throughout this book for the metastable β alloys.

The characteristic feature of the β alloys is that they do not transform martensitically upon fast cooling from the β phase field. The two alloys on top of the list in Table 2.6, Ti-6246 and Ti-17, are usually found in the group of α+β alloys [2.7, 2.24]. For the Ti-6246 alloy it was recently shown at the Technical University Hamburg-Harburg that all apparent martensite was attributable to artifacts introduced during normal specimen preparation, e.g. stress induced martensite by mechanical polishing for light microscopic and X-ray investigations or thin foil effects in case of TEM observations. There are numerous possibilities to form artifacts in titanium alloys during specimen preparation as will be discussed in more detail in Sects. 3.9.1 and 3.9.2. When the surface layer influenced by mechanical polishing was removed completely by electrolytic polishing, no martensite was found in the Ti-6246 alloy investigated (see Sect. 3.9.1, Fig. 3.79). This material was obtained from an alloy heat containing about 0.10% oxygen. In contrast, heats containing 0.15% oxygen have been reported to form α" martensite during quenching. Based on X-ray diffraction results, this α" martensite was concluded to be a bulk transformation product. For Ti-17, which contains more β stabilizers than Ti-6246, there exists strong evidence in the literature [2.25] that this alloy does not transform martensitically. Common to all β alloys is that relatively fast cooling from the β phase field and aging in the temperature region of about 500-600°C results in yield stress levels in excess of 1200 MPa. This high yield stress is due to the homogeneous precipitation of fine α platelets from the metastable precursor phases, ω or β', which are formed either during the cooling process to room temperature or during subsequent heating to the aging temperature (see Sect. 2.8.2). By comparison, the maximum yield stress level which can be obtained for α+β alloys, using the same cooling rates and optimum aging treatments, is only about 1000 MPa. This is because relatively coarse α plates form during the cooling process. These coarse α plates are either arranged in colonies or form as individual plates depending on alloy type, as pointed out earlier in Sect. 2.6.2.

Although the number of commonly used β titanium alloys in Table 2.6 is as large as the number of α+β alloys, it should be kept in mind, that the percentage of β alloy usage on the total titanium market is very low, (see Sect. 1.4). However, this percentage of β alloy usage is steadily increasing due to the attractive properties, especially the high yield stress level and for some applications (e.g. springs) the low modulus of elasticity.

2.8 Basic Hardening Mechanisms

From the four different hardening mechanisms in metallic materials (solid solution hardening, strengthening by a high dislocation density, boundary hardening, and precipitation hardening) solid solution and precipitation hardening are present in all commercial titanium alloys and should be discussed separately for the α phase (Sect. 2.8.1) and for the β phase (Sect. 2.8.2). Boundary hardening plays a significant role in α+β alloys cooled at high rates from the β phase field reducing the α

colony size to a few α plates or causing martensitic transformation. In both cases, a high dislocation density is created which also contributes to hardening. It should be pointed out, however, that the martensite in titanium is much softer than the martensite in Fe-C alloys because the interstitial oxygen atoms only cause small elastic distortion of the hexagonal lattice of the titanium martensite. This is in sharp contrast to carbon and nitrogen that cause severe tetragonal distortion of the bcc lattice in ferrous martensite.

2.8.1 Hardening of the Alpha Phase

The α phase is significantly hardened by the interstitial element oxygen. This can best be seen by comparing the yield stress values of the CP titanium grades 1-4 with oxygen levels between 0.18 and 0.40% (Table 2.6). By this increase in oxygen content the yield stress is increased from 170 MPa (grade 1) to 480 MPa (grade 4). In commercial titanium alloys the oxygen content varies between about 0.08% and 0.20% depending on alloy type. Substitutional solid solution hardening of the α phase is caused mainly by the elements Al, Sn, and Zr which have fairly large atomic size differences to titanium and also large solid solubilities in the α phase.

Precipitation hardening of the α phase occurs by coherent Ti_3Al particles above about 5% Al, see Ti-Al phase diagram in Fig. 2.11. These Ti_3Al or α_2 particles have an ordered hexagonal structure, crystallographically a DO_{19} structure, and since they are coherent, they can be sheared by moving dislocations resulting in planar slip and extensive dislocation pile-ups against boundaries. With increasing size, these α_2 particles become ellipsoidal in shape, the long axis being parallel to the c-axis of the hexagonal lattice [2.26]. This α_2 phase is further stabilized by the elements oxygen and tin, i.e. the $(\alpha+\alpha_2)$ phase region is pushed to higher temperatures by these elements. In such cases, Sn substitutes for Al whereas oxygen remains as an interstitial.

Upon annealing of α+β alloys in the two phase region (α+β), significant alloy element partitioning takes place and the α phase is enriched in α stabilizing elements (Al, O, Sn). Substantial volume fractions of coherent α_2 particles can then be precipitated in the α phase by aging for example at 500°C (Ti-6Al-4V, IMI 550), at 550°C (IMI 685), at 595°C (Ti-6242), or even at 700°C (IMI 834). The very high density of these homogeneously distributed α_2 particles in the α phase is shown in the dark field transmission electron micrograph in Fig. 2.20 for the IMI 834 alloy.

A change from wavy to planar slip is found in pure α titanium with increasing oxygen content [2.27], similar to that observed for microstructures containing coherent α_2 precipitates,. This observation might indicate that the oxygen atoms are not distributed homogeneously but tend to form zones with short range order. Also, a synergy between oxygen and Al atoms with regard to promoting planar slip has been demonstrated.

Although it has limited relevance to commercial titanium alloys, it should be mentioned that aging of the modulated microstructure, which results from the spinodal decomposition of the orthorhombic α" martensite (see Sect. 2.6.1), leads

to a drastic increase in yield stress [2.5]. This modulated structure can be considered as an array of very small, closely spaced precipitates. In this case, the disordered, solute rich zones become stronger obstacles to dislocation motion as their size and misfit increase with aging. Due to the large volume fraction of these zones in those modulated microstructures, the material becomes brittle on a macroscopic scale. The reason is the intense strain localization that occurs in this microstructure because the modulated zones are destroyed within the slip bands. This leads to the effect that the first slip band in the largest α" martensite plate develops sufficient strain to cause crack nucleation at the plate boundary. The fracture mechanism is microvoid coalescence and growth, not cleavage [2.5].

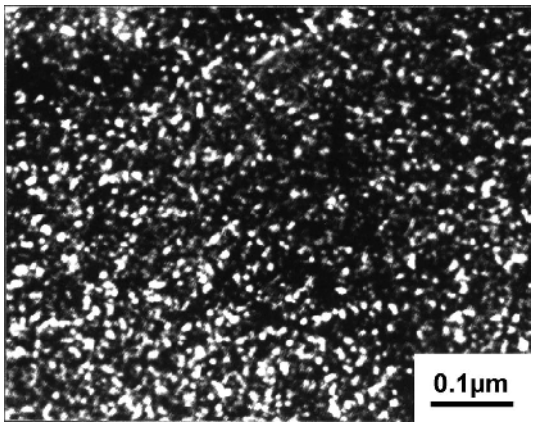

Fig. 2.20. Dark field micrograph of α_2 particles in IMI 834 aged 24 h at 700°C, TEM

2.8.2 Hardening of the Beta Phase

It is difficult to analyze solid solution strengthening of the β phase in a traditional sense because in fast cooled metastable β alloys the precursors of the metastable ω and β' phases cannot be separated from the solute effects. Also, in fully aged microstructures it is difficult to separate the hardening due to α precipitates from the solute effects. In this case, an important solid solution strengthening effect of the β phase is due to alloy element partitioning that accompanies α precipitation. One way to estimate the solid solution strengthening of the β stabilizing elements Mo, V, Nb, Cr, and Fe is to examine the slope of the lattice parameters versus solute content curves for binary alloys pointing out in a qualitative way the size misfit parameter. Data of this type can be found in Pearson's Handbook [2.28]. From this data it can be seen that the steepest slope is present for Ti-Fe followed by Cr and V, with Nb and Mo having a smaller effect on the lattice parameter.

Precipitation hardening of the β phase is the most effective way to increase the yield stress of commercial β titanium alloys. There are two metastable phases, ω

and β', which are observed in β titanium alloys as shown by the schematic phase diagram in Fig. 2.21 [2.29]. In both cases, it is a miscibility gap into two bcc phases, β_{lean} and β_{rich}, the major difference being the magnitude of distortion of the bcc lattice in the coherent disordered precipitates (β_{lean}) with respect to the bcc lattice of the matrix (β_{rich}). In highly concentrated alloys the magnitude of distortion is very small and the metastable particles are called β' having a bcc crystal structure. In case of less concentrated alloys the distortion of the bcc lattice in the precipitates is much higher and the metastable particles are called isothermal ω having a hexagonal crystal structure from a crystallographic viewpoint (see discussion on athermal ω in Sect. 2.6.1 and Fig. 2.16).

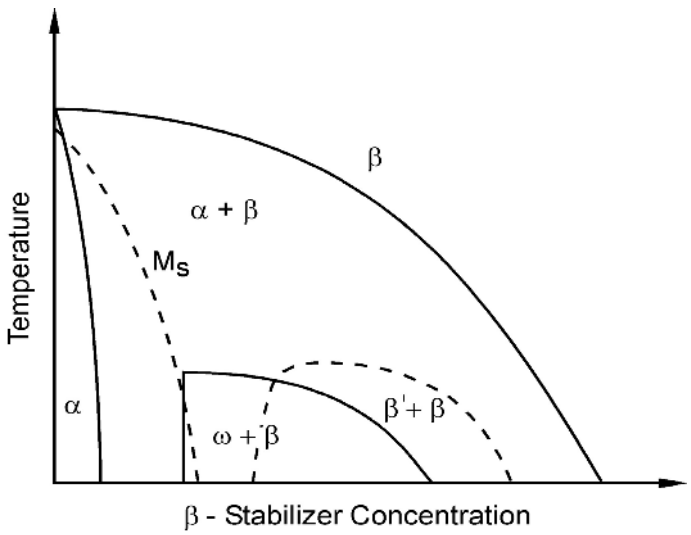

Fig. 2.21. Metastable (ω+β) and (β'+β) phase fields in a β isomorphous phase diagram (schematically)

The isothermal ω particles have either an ellipsoidal or a cuboidal shape depending on the precipitate/matrix misfit [2.30]. At low misfits, the ω particles are ellipsoidal with the long axis being parallel to one of the four <111> directions of the bcc lattice. An example is shown in the dark field micrograph in Fig. 2.22 imaging one of the four variants of the ellipsoidal ω particles in a Ti-16Mo alloy aged 48 h at 450°C. At larger misfits, the ω particles become cuboidal with the flat surfaces being parallel to the {100} planes of the bcc lattice. An example is shown in Fig. 2.23 for a Ti-8Fe alloy aged 4 h at 400°C.

The β' precipitates have a morphology which varies from spheres or cuboids in Ti-Nb and Ti-V-Zr alloys to plates in Ti-Cr alloys [2.30], again depending on the magnitude of misfit and coherency strains. One example for the solute lean β' precipitates is shown in Fig. 2.24 for the Ti-15Zr-20V alloy aged 6 h at 450°C.

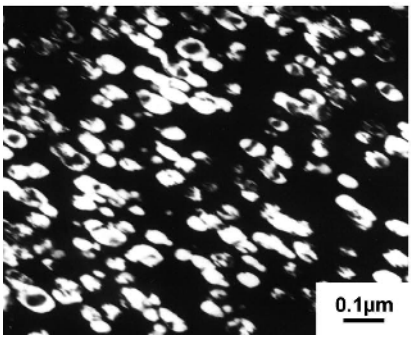

Fig. 2.22. Dark field micrograph of ellipsoidal ω precipitates in Ti-16Mo aged 48 h at 450°C, TEM

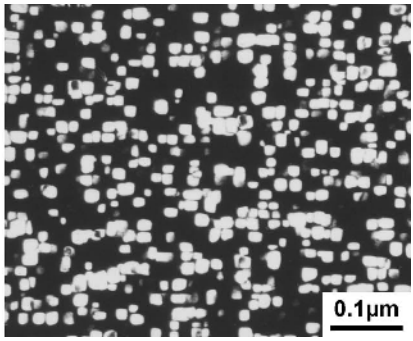

Fig. 2.23. Dark field micrograph of cuboidal ω precipitates in Ti-8Fe aged 4 h at 400°C, TEM

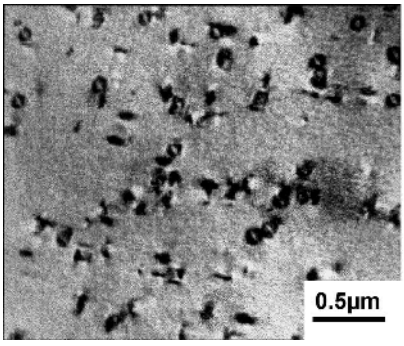

Fig. 2.24. Coherent β' particles in Ti-15Zr-20V aged 6 h at 450°C, TEM

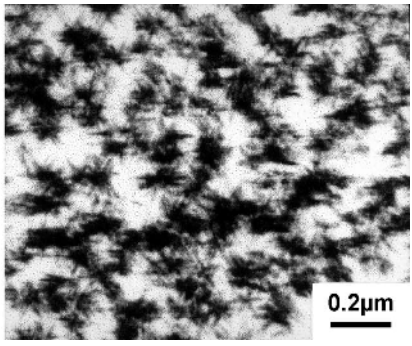

Fig. 2.25. Precipitation of small α platelets at β' particles in Ti-15.6Mo-6.6Al aged 100 h at 350°C, TEM

Both ω and β' are coherent and are sheared by the moving dislocations. This results in the formation of intense, localized slip bands leading to early crack nucleation and low ductility [2.31]. Therefore, microstructures containing these precipitates are usually avoided in commercial β titanium alloys. Instead, commercial β titanium alloys are aged at slightly higher temperatures in order to precipitate in reasonable aging times incoherent particles of the stable α phase using ω or β' particles as precursors and nucleation sites. Sometimes it is necessary to use a step aging treatment as will be discussed in more detail at the end of this section. Using these precursors, it is possible to obtain a fairly homogeneous distribution of small α platelets. An example of the early stages of α nucleation is shown in Fig. 2.25 for Ti-15.6Mo-6.6Al aged for a long time (100 h) at 350°C [2.29]. The size and distribution of α platelets in a commercial β titanium alloy, the β-CEZ alloy de-

veloped by CEZUS in France, with the recommended aging treatment of 8 h at 580°C is shown in Fig. 2.26. These α platelets also obey the Burgers relationship and the flat surface of the platelets is parallel to one of the {112} planes of the β matrix, as described in Sect. 2.6.2, see also Fig. 2.18. As pointed out already in that section and as can be seen in Fig. 2.26, not all twelve possible variants are nucleated statistically. Instead, in order to minimize the overall elastic strains only two or three variants being nearly perpendicular to each other dominate in a given volume of a β grain.

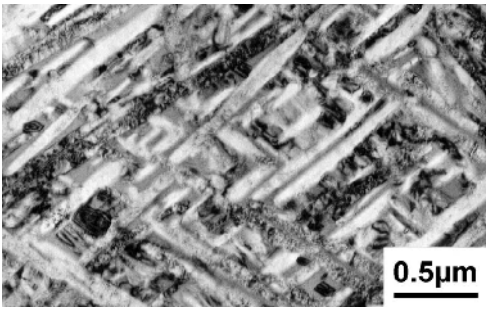

Fig. 2.26. Size and distribution of α platelets in the commercial β titanium alloy β-CEZ aged 8 h at 580°C, TEM

Since these incoherent α platelets are too small to deform plastically they act as hard, undeformable particles. Consequently, high yield stresses can be obtained in β titanium alloys with such microstructures. The yield stress in those alloys can be easily lowered, i.e. adjusted to the desired level, by applying a two-stage heat treatment. In this case, the first annealing step is done at high temperatures in the (α+β) phase field to precipitate a desired volume fraction of large α plates and reducing thereby the volume fraction of small α platelets in the second aging step at lower temperature. The large α plates contribute less to the yield stress than the small α platelets because they are large enough to deform plastically and only boundary hardening is present as a hardening mechanism for the large α plates. However, for all microstructures with α precipitates the dislocation density increases in the β matrix during α precipitation. Therefore, dislocation hardening is also contributing to the yield stress.

It was already pointed out in Sect. 2.6.2 that the α phase always nucleates preferentially at β grain boundaries forming continuous α layers. Especially for β alloys, hardened by small α platelets to high yield stress levels, these continuous α layers become deleterious to the mechanical properties. An example of such a microstructure is shown in Fig. 2.27 for the β alloy Ti-10-2-3. The main intention of the thermo-mechanical processing of β alloys is to eliminate or reduce this negative effect of the continuous α layers on mechanical properties (see Sect. 7.1).

In β alloys with high concentrations of β stabilizing elements it is sometimes difficult to achieve a homogeneous distribution of α platelets by normal aging

treatments, especially with aging temperatures above the metastable two phase region, because the formation of precursors (ω or β') or α nucleation at the precursors is too sluggish to occur during the heating period to the aging temperature. In such a case, a pre-aging treatment at lower temperature might create a more homogeneous distribution of α platelets, as shown in Fig. 2.28 for the β alloy Beta C [2.32]. Another possibility is to cold work prior to aging which results in a more homogeneous distribution of α platelets by nucleation at dislocations.

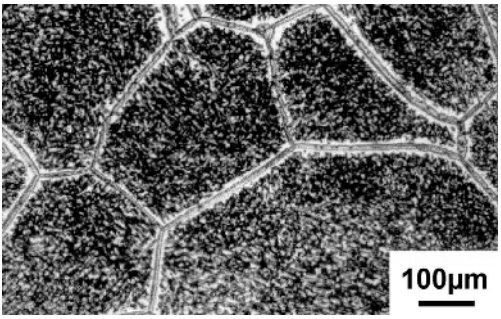

Fig. 2.27. Continuous α layers at β grain boundaries in the β alloy Ti-10-2-3, LM

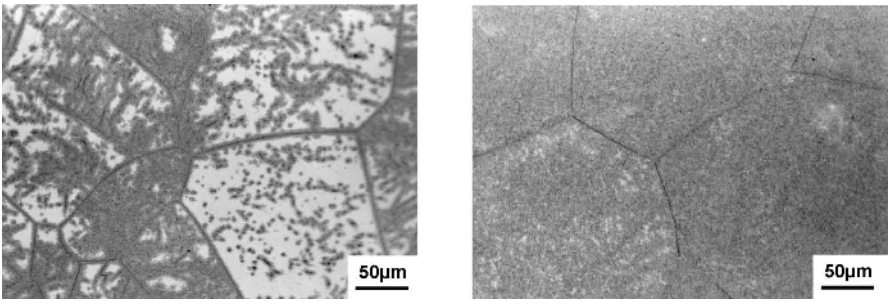

a **b**

Fig. 2.28. Effect of pre-aging on distribution of α platelets in the β alloy Beta C, LM: (a) 16 h 540°C (b) 4 h 440°C + 16 h 560°C

2.9 Basic Physical and Chemical Properties

For most application purposes the majority of physical and chemical properties of titanium are far less important than the mechanical properties. Noteworthy exceptions are the low density and the formation of the surface oxide layer which imparts very good corrosion resistance. Most of the properties will be discussed in

general terms, only a few of them will be treated in some detail. Among these are diffusion (Sect. 2.9.1), corrosion behavior (Sect. 2.9.2), and oxidation (Sect. 2.9.3). The modulus of elasticity was discussed already in Sect. 2.3.

In addition to the basic characteristics, already shown in Table 2.1, other selected physical properties of titanium and its alloys are listed in Table 2.7 [2.7]. These are compared to other metallic structural materials. The property values for high purity α titanium shown in Table 2.7 are not significantly different than those for the various CP titanium grades. This shows that oxygen concentrations up to 0.40% only slightly affect these properties. On the other hand, if the values for the α+β alloy Ti-6Al-4V and for the β alloy Ti-15-3 are compared with those of pure α titanium, it can be seen that the thermal conductivity and the electrical resistivity vary significantly. Thermal conductivity is lower and electrical resistivity is higher for these commercial alloys, whereas the linear expansion coefficient and the specific heat capacity are only slightly affected. The thermal conductivity and the electrical resistivity both depend on the density and extent of scattering of the conductive electrons. The increase in electrical resistivity with increasing solute content in binary titanium alloys is shown in Fig. 2.29 [2.6]. It can be seen that there are two branches in the dependency, the upper branch contains the elements which show the tendency for ordering in α titanium and the lower branch consists of the elements showing the tendency for inmiscibility (V, Nb) or behaving completely neutral (Zr). It should be pointed out, that oxygen belongs to the upper branch because the electrical resistivity of CP titanium grade 4 with 0.40% oxygen is 0.60 μΩ m (thermal conductivity: 17 W m^{-1} K^{-1}). In addition to the electrical resistivity of titanium alloys described in Table 2.7, a number of β titanium alloys have been shown to exhibit superconducting behavior. This behavior will be addressed in this book in Chap. 10 (Special Properties and Applications of Titanium).

Table 2.7. Some physical properties of titanium and its alloys as compared to other structural metallic materials

	Linear Thermal Expansion Coefficient (10^{-6} K^{-1})	Thermal Conductivity (W m^{-1} K^{-1})	Specific Heat Capacity (J kg^{-1} K^{-1})	Electrical Resistivity (μΩ m)
α Titanium	8.4	20	523	0.42
Ti-6Al-4V	9.0	7	530	1.67
Ti-15-3	8.5	8	500	1.4
Fe	11.8	80	450	0.09
Ni	13.4	90	440	0.07
Al	23.1	237	900	0.03

Comparing the values for titanium with those of other structural metallic materials it can be seen that the linear thermal expansion coefficient is lower for titanium. Consequently, titanium alloys are an excellent choice for applications re-

quiring a high strength to density ratio and a low thermal expansion. Examples include casings for aero-engines and connecting rods in automobile engines. Unfortunately due to the high price of titanium, the application as connecting rods is limited to high performance, high-priced vehicles. It also should be pointed out, that the linear thermal expansion coefficient for α titanium is about 20% higher parallel to the c-axis than perpendicular to the c-axis. This becomes important if highly textured Ti-6Al-4V material is used as connecting rod material.

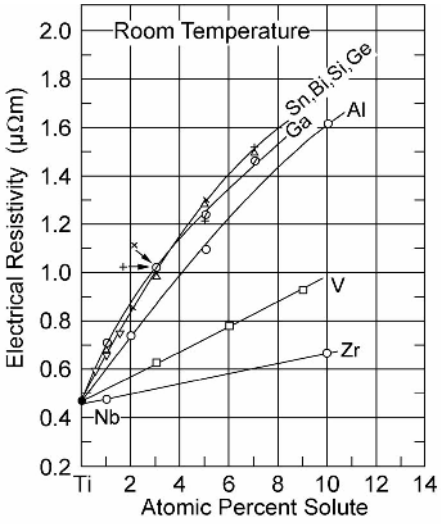

Fig. 2.29. Electrical resistivity of binary titanium alloys [2.6]

The thermal conductivity of titanium is significantly lower as compared to Fe, Ni, and Al (Table 2.7) which affects for example the obtainable cooling rates after processing and heat treatments, as well as the heating times. The high electrical resistivity of titanium as compared to the other metals in Table 2.7 limits the usefulness of titanium as an electrical conductor. The specific heat capacity of titanium has the same order of magnitude as the other metals listed in Table 2.7.

The strength to density advantage of titanium compared to other structural metallic materials was already illustrated in Table 2.1 for typical α+β titanium alloys (yield stress 1000 MPa, density 4.5 g cm^{-3}). This advantage is not significantly increased for high strength β alloys with typical yield stress values of 1200 MPa, because most β alloys contain heavy elements like Mo and the density of those alloys is increased by about 5% and can be as high as 4.94 g cm^{-3} in the case of the β alloy Beta 21S.

2.9.1 Diffusion

Knowledge of the diffusion rates of interstitial and substitutional alloying elements in the α and β phases of titanium, as well as the self-diffusion rates, is important. Many of the production processes, such as solution and aging heat treatments, hot working, and recrystallization temperatures, are diffusion dependent. So are many application aspects, for example creep, oxidation behavior, and hydrogen embrittlement.

Many diffusivity data were measured especially during the first twenty years of commercialization of titanium and these data are well documented in the German titanium book by Zwicker in 1974 [2.33]. The intrinsic problem of scatter in the diffusion data, partially due to the measurement method used, was pointed out by Liu and Welsch in their literature survey on diffusivities of oxygen, aluminum, and vanadium in α and β titanium in 1987 [2.34], done probably with respect to the widely used Ti-6Al-4V alloy. In a recently published overview article [2.35], new diffusivity data as well as improvements in the understanding of diffusivities, especially for the α phase, are presented.

A selection of diffusivity data is shown in Fig. 2.30 in the form of Arrhenius plots. It can be seen that the self-diffusion of titanium in the β phase is about three orders of magnitude faster than the self-diffusion in the α phase (β-Ti and α-Ti lines in Fig. 2.30). The diffusion rates of substitutional elements in the β phase can be either slower or faster than the self-diffusion of titanium [2.33]. From the group of slow diffusing elements, Al and Mo are shown as examples in Fig. 2.30. Among the other important alloying elements belonging to this group, V and Sn are close to Al, and Nb lies in between Al and Mo. Among the group of fast diffusing elements, Fe is shown as an example in Fig. 2.30. Ni is even slightly faster, whereas Cr and Mn fall in between Fe and the β-Ti self-diffusion line. From the various diffusion rates measured for oxygen in β titanium, the upper set of curves, shown in [2.34], is taken for Fig. 2.30 because, as pointed out in [2.34], the slope (activation energy) of the lower set of curves seems to be too high.

From the diffusivity data for α titanium, the results obtained for oxygen all show reasonable agreement [2.34], and the line shown in Fig. 2.30 seems to be well established. Only a limited number of diffusivity measurements for aluminum in α titanium exists and, apart from the scatter, most of these data lie close to the oxygen line in Fig. 2.30 [2.34]. This is unusually high for substitutional elements. It is well established that the group Fe, Ni, and Co exhibits an abnormally high diffusivity in α titanium (see Fe line in Fig. 2.30). This is explained by an interstitial diffusion mechanism of these elements [2.35]. This fast interstitial diffusion mechanism also increases the vacancy diffusion rate for self-diffusion and Al in α titanium, if the measurements are done on materials with normal Fe impurity content [2.35]. Measurements on ultrahigh purity α titanium with respect to Fe, Ni, and Co impurities [2.35] resulted in very low diffusivity rates for self-diffusion and Al in α titanium (Fig. 2.30) being characteristic of vacancy controlled diffusion. Besides Al, the elements Zr, Hf, Au, In, and Ga are also normal diffusing elements (vacancy mechanism) and their diffusivities are close to the Al line in Fig. 2.30. Cr and Mn probably belong as Fe, Ni, and Co to the fast diffu-

sion elements (interstitial mechanism) although their diffusivity is about two orders of magnitude slower than Fe, Co, and Ni. According to [2.35], this is still much too fast for a vacancy mechanism.

It should be emphasized once more, that the diffusivity data of substitutional elements in α titanium apparently depend strongly on the Fe impurity level of the material. For commercial titanium alloys, this effect is particularly important for the diffusion of aluminum in the α phase.

The interstitial element hydrogen exhibits very high diffusion rates in the β phase as well as in the α phase (Fig. 2.30), which has serious consequences for applications of titanium alloys in aqueous or humid gaseous environments, especially under high static loads (stress corrosion cracking) or fatigue loading (corrosion fatigue), because of hydrogen embrittlement.

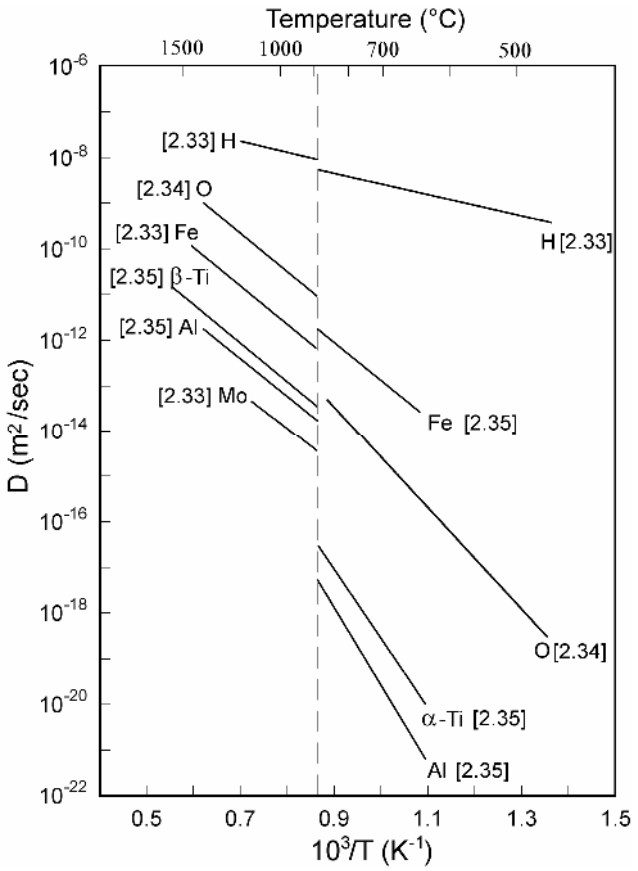

Fig. 2.30. Arrhenius diagram of titanium self-diffusion and various alloying elements in the β and α phases of titanium (dashed line: β to α transformation temperature)

2.9.2 Corrosion Behavior

In the galvanic series of metals, titanium has a standard potential of −1.63 V which is close to aluminum. Therefore, titanium cannot be considered as being intrinsically noble. Yet, the excellent resistance of titanium to general corrosion in most environments is well-known. This is the result of a stable protective surface film, which consists basically of TiO_2. This thin oxide film passivates titanium as long as the integrity of the film is maintained. In general, this is the case in most oxidizing environments, for example in salt solutions, including chlorides, hypochlorites, sulfates, and sulfites, or in nitric and chromic acid solutions. On the other hand, titanium is not corrosion resistant under reducing conditions, where the protective nature of the oxide film breaks down. Consequently, the corrosion resistance of titanium in reducing environments, such as sulfuric, hydrochloric, and phosphoric acids, is not good [2.36]. For example, titanium dissolves very rapidly in hydrofluoric acid, mainly because this acid causes the oxide film to break down, exposing reactive metallic titanium. This is why a $HF\text{-}HNO_3$ mixture is used to chemically mill and to pickle titanium during its production. In many commercially used reducing environments, the stability and integrity of the protective titanium oxide film can be improved by adding inhibitors (oxidizing agents) to these environments [2.36].

Passivated titanium is very corrosion resistant in flowing seawater at room temperature and in this environment has a potential close to that of Hastelloy, Inconel, Monel, and passive austenitic stainless steels [2.37]. In addition, titanium normally does not contain inclusions such as oxides, carbides, and sulfides. Therefore, titanium has a much greater resistance to pitting corrosion than the materials just mentioned.

The good general corrosion resistance of unalloyed titanium is also observed for $\alpha+\beta$ and β alloys. From an economic standpoint (cost, formability, weldability) CP titanium grades are preferred in applications that do not require higher strength levels. The corrosion resistance of CP titanium grade 2 in reducing acids can be improved significantly by small additions of noble metals, such as 0.2% Pd, grade 7 (Table 2.6), or to a smaller extent by adding 0.3% Mo+0.8% Ni, grade 12 (Table 2.6). This is shown in Table 2.8, where CP titanium grade 2 and the alloy grades 7 and 12 are compared with respect to the acid concentration limits resulting in a corrosion rate of about 125 μm/year [2.38]. Table 2.8 represents a summary of data acquired by Covington and Schutz, TIMET. A more detailed coverage of these data can be found in the Metals Handbook [2.36]. The data in Table 2.8 show that the highest acid concentration limit in all three acids is obtained for grade 7 with 0.2% Pd, followed by grade 12, and then by CP titanium grade 2. The addition of 0.2% Pd shifts the corrosion potential in the acids towards the increasingly noble (positive) direction, where the protective surface oxide film is stable, and full passivity can be achieved in dilute reducing acids [2.39].

The resistance to general corrosion of the higher strength $\alpha+\beta$ and β titanium alloys has been evaluated in a reducing acid environment by Schutz [2.40]. These results show that alloy contents of more than 3% Mo and 8% Zr are exceptionally beneficial, vanadium is of minor importance, but Al levels above 3% are increas-

ingly detrimental. Table 2.9 shows the active-to-passive transition acid concentrations in boiling HCl at a corrosion rate of about 125 μm/year for the α+β alloy Ti-6Al-4V and for various β alloys. It can be seen that the β alloy Beta 21S with 15% Mo exhibits the best corrosion resistance in reducing acid environments, but some of the advantage is lost if used in the high strength aged condition.

Table 2.8. Acid concentration limits (wt%) for CP titanium grade 2 and alloy grades 7 and 12 in reducing acids for a corrosion rate of about 125 μm/year [2.38]

Acid	Temperature	Grade 2	Grade 7	Grade 12
HCl	24°C	6	25	9
	Boiling	0.6	4.6	1.3
H_2SO_4	24°C	5	48	10
	Boiling	0.5	7	1.5
H_3PO_4	24°C	30	80	40
	Boiling	0.7	3.5	2

Table 2.9. Active-to-passive transition acid concentrations at a corrosion rate of about 125 μm/year for Ti-6Al-4V and various β alloys in boiling HCl [2.40]

Alloy	Annealed Condition (% HCl)	Aged Condition (% HCl)
Ti-10-2-3	-	0.08
B120VCA	0.10	-
Ti-15-3	0.12	0.08
Ti-6-4	0.12	0.13
Beta C	1.1	0.87
Beta 21S	5.0	1.5

The resistance to pitting corrosion of titanium is generally very high because of its protective oxide film and, as already mentioned, the virtual absence of inclusions. The resistance to pitting is measured electrochemically either by the anodic breakdown potential or by the repassivation potential [2.36]. A comparison of the repassivation potential (also known as critical pitting potential, E_{pit}) between CP titanium and various titanium alloys in boiling 5% NaCl solution is shown in Table 2.10 [2.40]. It can be seen that CP titanium exhibits the highest value (6.2 V) and has therefore, in this comparison, the highest resistance to pitting corrosion. Although the potential values are lower for all titanium alloys listed in Table 2.10, the titanium alloys are still considered to be resistant to pitting corrosion because the repassivation potential values are higher than 1 V [2.36]. The values in Table 2.10 show that some β alloys, including Beta C and Beta 21S, exhibit a better resistance to pitting corrosion than the α+β alloy Ti-6Al-4V.

Crevice corrosion is often the critical mode of attack for titanium in chloride, fluoride, or sulfate containing solutions when temperatures exceed 75°C. Within

crevices oxygen depleted reducing acid conditions can develop with pH values as low as 1 or below, because of the small and restricted volume of solution involved. Figure 2.31 illustrates the combination of pH level and temperature at which crevice attack is observed for various titanium grades (Table 2.6) in NaCl-rich brines [2.36]. It can be seen that the crevice corrosion resistance of CP titanium grade 2 can be improved by adding 0.3Mo+0.8Ni (grade 12) or even more by the addition of Pd (grade 7). The resistance to crevice corrosion of Ti-6Al-4V is similar to that of CP titanium grade 2, whereas the β titanium alloys Beta C and Beta 21S show a better resistance to crevice corrosion in most aggressive environments [2.40]. A further discussion of the relation between environmental effects and alloy performance in specific applications is included in Sect. 4.2 of the chapter "Commercially Pure (CP) Titanium and Alpha Alloys".

Table 2.10. Repassivation potential (also known as critical pitting potential, E_{pit}) in boiling 5% NaCl solution of CP titanium, Ti-6Al-4V, and various β alloys in the annealed condition [2.40]

	CP-Ti Grade 2	Ti-6-4	Ti-15-3	B120VCA	Beta 21S	Beta C
Repassivation Potential (V) vs. Ag/AgCl	6.2	1.8	2.0	2.7	2.8	3.0

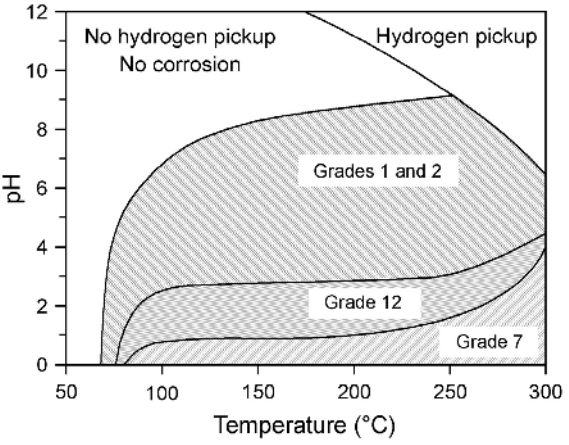

Fig. 2.31. Temperature and pH limits for crevice corrosion of various titanium grades in NaCl-rich brines (attack in shaded areas) [2.36]

The combination of corrosive environment and applied stress can cause the degradation of some important mechanical properties. The tensile ductility can be reduced if crack nucleation is shifted to the specimen surface, cracks connected to

the surface can propagate under constant load conditions (stress corrosion cracking), and in fatigue loading surface cracks can nucleate and propagate at lower stress amplitudes as compared to inert environment (corrosion fatigue). The magnitude of these effects will be shown and discussed in this book in the relevant materials sections, for example for α+β alloys in Chap.5. The present discussion will be limited to a brief description of the basic mechanism which is responsible for the above mentioned effects.

Hydrogen is the fastest diffusing element (Fig. 2.30) and the most detrimental acting environmental species in combination with an applied stress (hydrogen embrittlement). In general, there are two possible sources for hydrogen, the internal hydrogen of the material or external hydrogen from the environment. The negative effects due to internal hydrogen are well under control in titanium by strictly limiting the maximum hydrogen content in CP titanium and titanium alloys to 125-150 ppm. Still, hydrogen related problems can occur in the presence of sharp notches, as will be discussed in Chap. 4.

The external hydrogen from the environment can be swept into the material interior by moving dislocations if the slip steps at the surface are higher than the thickness of the protective oxide layer. In this way, the hydrogen concentration within the slip bands can locally reach such a high level that the fracture stress within the slip bands is reduced leading to easier crack nucleation and crack propagation. For the hexagonal α phase, it is observed that this hydrogen induced fracture preferentially takes place on the basal planes. Therefore, a pronounced effect of crystallographic texture on the magnitude of degradation of the relevant mechanical properties is observed for α+β titanium alloys (Sect. 5.2.6). The reason for the preferred fracture along basal planes is still unknown. In contrast to α and α+β alloys, β titanium alloys are less sensitive to hydrogen embrittlement especially in the annealed condition. This beneficial behavior is somewhat reduced for the aged condition with a higher volume fraction of α phase. This higher tolerance of β alloys to hydrogen is attributed to the bcc crystal structure of the β matrix and to the higher solid solubility of hydrogen in the β phase as compared to the α phase.

2.9.3 Oxidation

The oxidation product of titanium during exposure to air is TiO_2 which has a tetragonal rutile crystal structure. This oxide layer is often called scale and is an n-type anion-defective oxide, through which the oxygen ions can diffuse. The reaction front is at the metal/oxide interface and the scale grows into the titanium base material. The driving force for the rapid oxidation of titanium is the high chemical affinity of titanium to oxygen which is higher than for titanium and nitrogen. During the oxidation process, the high affinity of titanium to oxygen and the high solid solubility of oxygen in titanium (about 14.5%) results in the simultaneous formation of the scale and an adjacent oxygen rich layer in the base metal. This oxygen rich layer is called α-case because it is a continuous layer of oxygen stabilized α phase. As mentioned in Sect. 2.8.1, an increasing oxygen level strengthens the α phase and changes the deformation behavior of α titanium from a wavy to a

planar slip mode. Therefore, the hard, less ductile α-case can result in the formation of surface cracks under tension loading. The low local ductility and the large slip offsets at the surface can cause low overall ductility or early crack nucleation under fatigue loading conditions. The high temperature application of conventional titanium alloys is therefore limited to a temperature regime below about 550°C. The diffusion rates through the scale (oxide layer) below 550°C are slow enough to prevent excess oxygen contents being dissolved in the bulk material, resulting in no significant α-case formation.

In order to decrease the diffusion rate of oxygen through the scale, various additions of alloying elements have been investigated [2.33]. Improvements were found by adding Al, Si, Cr (> 10%), Nb, Ta, W, and Mo. These elements form either thermally stable oxides (Al, Si, Cr) or have a valency greater than four, for example Nb^{5+}. By substituting for the Ti^{4+} ions in the TiO_2 structure niobium reduces the number of anion vacancies and therefore reduces the oxygen diffusion rate. Based on this effect, a β titanium sheet alloy (Beta 21S) with the composition Ti-15Mo-2.7Nb-3Al-0.2Si (see Table 2.6) was developed [2.41]. This β alloy has a higher oxidation resistance but a lower high temperature strength and creep resistance than the α+β high temperature alloys Ti-6242 and IMI 834. However, increasing amounts of aluminum are much more effective in lowering the diffusion rates, because aluminum forms a dense and thermally stable α-Al_2O_3 oxide. The resulting scale consists of a heterogeneous mixture of TiO_2 and Al_2O_3 underneath the TiO_2 surface oxide layer, as shown schematically in Fig. 2.32 [2.42].

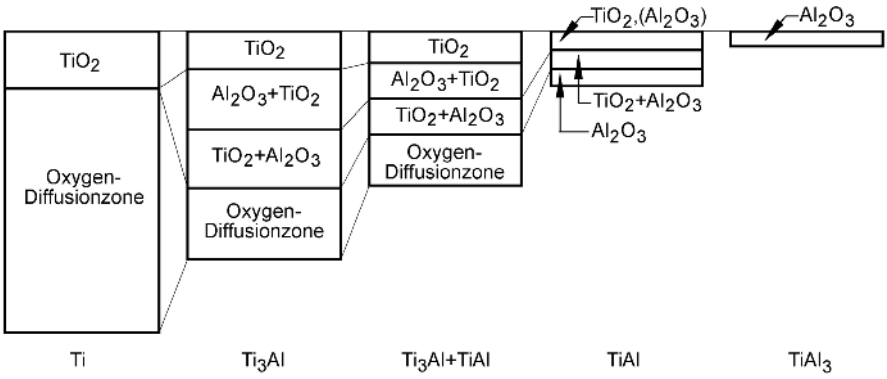

Fig. 2.32. Schematic cross sections through the oxide layers and the oxygen diffusion zone in titanium and titanium-aluminides [2.42]

The improved oxidation resistance of titanium aluminides, such as Ti_3Al or γ-TiAl based alloys, results from an increased volume fraction of Al_2O_3 in the scale (Fig. 2.32). The amount of Al_2O_3 increases with aluminum concentration and the Al_2O_3 layer becomes continuous around 40 at% Al. Consequently, γ-TiAl exhibits a better oxidation resistance than alloys based on Ti_3Al. This is because TiO_2 is not stable on titanium alloys at high temperatures and the Al_2O_3 layer is not con-

tinuous on Ti_3Al (Fig. 2.32), whereas the Al_2O_3 layer is continuous on γ-TiAl and stable up to much higher temperatures. This improved oxidation resistance can be used for the development of surface coatings for conventional titanium alloys, such as IMI 834, to allow application temperatures above 550°C. Many different coatings have been investigated, for example Pt, NiCr, Si, Si_3N_4, Al, MCrAlY, silicates, SiO_2, Nb [2.43], but the most promising results are obtained by sputtering Ti-Al coatings. This is shown in Fig. 2.33 for the high temperature alloy Ti-1100 [2.44]. Although this alloy is no longer produced by TIMET, the results are still useful, because Ti-1100 exhibits at 700°C a similar oxidation behavior as IMI 834 [2.45]. From Fig. 2.33 it can be seen that the Ti-Al coating produced a better oxidation resistance than Si or Pt coatings. Furthermore, the Ti-Al coated material exhibited a better oxidation resistance at 750°C than the uncoated material at 600°C.

A special case of oxidation resistance is the ignition and burn resistance. In normal atmospheric air environment, all titanium alloys are generally resistant to ignition and burning, but under special conditions, such as in gas turbine aero-engine compressors (high pressures, high air flow velocities), ignition and burning is possible for many titanium alloys [2.39]. This special case will be discussed in more detail in Chap. 10 (Special Properties and Applications of Titanium), together with some alloying approaches that have been used to mitigate this problem.

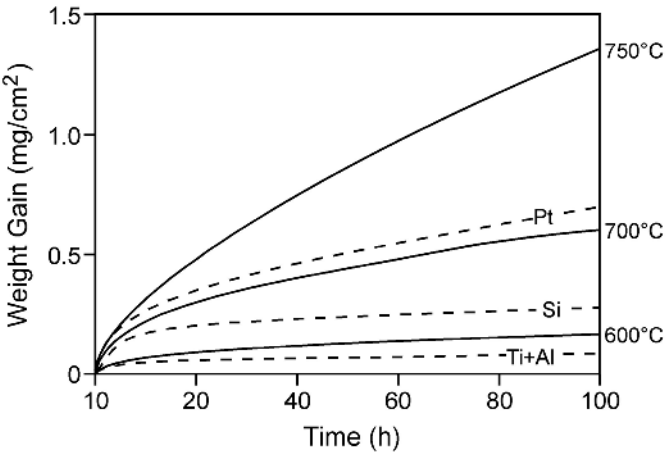

Fig. 2.33. Oxidation behavior of Ti-1100 material at different temperatures in comparison to coated material at 750°C (dashed curves) [2.44]